Current Photovoltaic Research 7(4) 103-110 (2019)
DOI:https://doi.org/10.21218/CPR.2019.7.4.103
pISSN 2288-3274
eISSN 2508-125X

Performance Improvement by Controlling Se/metal Ratio and Na_2S Post Deposition Treatment in $Cu(In,Ga)_3Se_5$ Thin-Film Solar cell

Hui-Ling Cui[1] · Seung Tae Kim[1] · R.B.V. Chalapathy[2] · Ji Hye Kim[3] · Byung Tae Ahn[1]*

[1]Department of Materials Science and Engineering, Korea Advanced Institute of Science and Technology, Daejeon 34141, South Korea
[2]Department of Physics, Vel Tech High Tech Dr Rangarajan Dr Sakunthla Engineering College, Chennai 600 062, India
[3]Isac Research, Daejeon, 34036, South Korea

Received September 17, 2019; Revised December 8, 2019; Accepted December 10, 2019

ABSTRACT: $Cu(In,Ga)_3Se_5$ (β-CIGS) has a band gap of 1.35 eV, which is an optimum value for high solar-energy conversion efficiency. The effects of Cu and Ga content on the cell performance were investigated previously. However, the effect of Se content on the cell performance is not well understood yet. In this work, β-CIGS films were fabricated by three-stage co-evaporation of elemental sources with various Se fluxes at the third stage instead of at all stages. The average composition of five samples was $Cu_{1.05}(In_{0.59},Ga_{0.41})_3Se_y$, where the stoichiometric y value is 5.03 and the stoichiometric Se/metal (Se/M) ratio is 1.24. We varied the Se/metal ratio in a range from 1.18 to 1.28. We found that the best efficiency was achieved when the Se/M ratio was 1.24, which is exactly the stoichiometric value where the CIGS grains on the CIGS surface were tightly connected and faceted. With the optimum Se/M ratio, we were able to enhance the cell efficiency of a β-CIGS solar cell from 9.6% to 12.0% by employing a Na_2S post deposition treatment. Our results indicate that Na_2S post deposition treatment is very effective to enhance the cell efficiency to a level on par with that in α-CIGS cell.

Key words: Thin-film solar cells, $Cu(In,Ga)_3Se_5$, β -CIGS, Se/metal ratio, Na_2S post deposition treatment

Nomenclature

η: conversion efficiency of solar cell, %
J_{sc}: short-circuit current, mA/cm^2
V_{oc}: open-circuit voltage, V
FF: fill factor, %
R_{sh}: shunt resistance, $\Omega \cdot cm^2$
R_s: series resistance, $\Omega \cdot cm^2$

Subscript

Se/M: Se/metal ratio
CGI: Cu/(Ga+In) ratio
GGI: Ga/(Ga+In) ratio
PDT: post deposition treatment

*Corresponding author: btahn@kaist.ac.kr

1. Introduction

$Cu(In,Ga)Se_2$ (α-CIGS) solar cells with a ban gap of 1.2 eV have received a great deal of attention due to their long-term stability in outdoor conditions and high absorption coefficient. The efficiency of α-CIGS solar cells is as high as 22.6-22.9%[1, 2].

The $Cu(In,Ga)_3Se_5$ (β-CIGS) phase is often found on the surface of the α-CIGS film because of excess supply of In, Ga, and Se during the three-stage co-evaporation process[3-5]. The existence of this phase greatly enhances the device performance of the CIGS solar cell[6, 7]. It is seen that an epitaxial surface layer with an intrinsic β-CIGS phase prevents surface recombination by reducing the valence band maximum downward at the CIGS surface.

β-CIGS material with a band gap of 1.34 eV has potential for higher efficiency than that of α-CIGS material with a band gap of 1.2 eV according to the Shockley-Queisser limit. However, the cell efficiency with a β-CIGS light absorber was below 15% even though the band gap of β-CIGS was favorable compared to α-CIGS light absorber.

Fig. 1 shows the tetragonal crystal structure of the β-CIGS

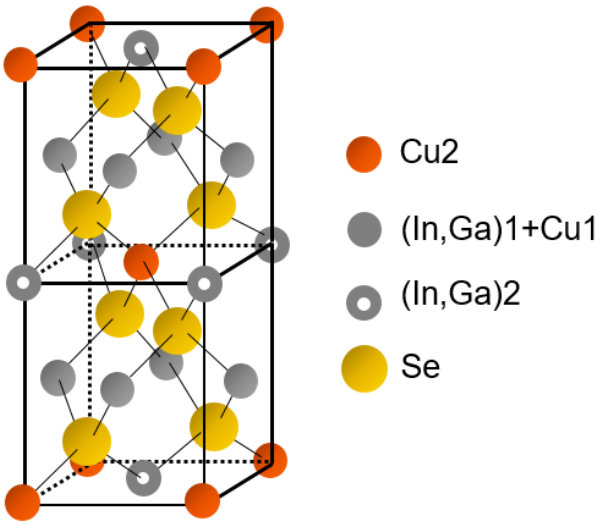

Fig. 1. Crystal structure of $Cu(In,Ga)_3Se_5$ (β-CIGS) phase (Paszkowicz model).

phase from Pasczkowicz model[8-10]. In the structure, the compound may contain ordered vacancies or no vacancies depending on the Se content.

As shown in Fig. 1, the appropriate composition corresponding to the structure is $Cu(In,Ga)_3Se_4$ because the unit cell contains two $Cu(In,Ga)_3Se_4$ molecules instead of two $Cu(In,Ga)_3Se_5$ molecules.

We suggest following two possible reactions for β-CIGS formation from Cu_2Se and $(In,Ga)_2Se_3$ phases.

$$Cu_2Se + 3\ (In,Ga)_2Se_3 \rightarrow 2\ Cu(In,Ga)_3Se_5 \quad (1)$$

$$Cu_2Se + (In,Ga)_2Se_3 + 4\ (In,Ga)Se \rightarrow 2\ Cu(In,Ga)_3Se_4 \quad (2)$$

The Se/metal (Se/M) ratios in equation (1) and equation (2) are 1.25 and 1.0, respectively. At this point, the most appropriate Se/M ratio for this material for application to a solar cell absorber has not been well understood. Therefore, controlling the Se amount might be very important in this film.

The band gap of β-CIGS material varies by the Cu content and Ga content in the material. Previously, we reported the effect of Cu and Ga content in β-CIGS phase on the characteristics and cell performance of a β-CIGS solar cell[11]. We also reported that the best efficiency was achieved when the Se flux was 16 Å/s to achieve cell efficiency of about 10%, suggesting that careful control of the amount of Se is very important[12].

In this paper, we maintained 14 Å/s flux in all the stages except the third stage where the flux was slightly modified to investigate the effect of Se content near the surface. Therefore,

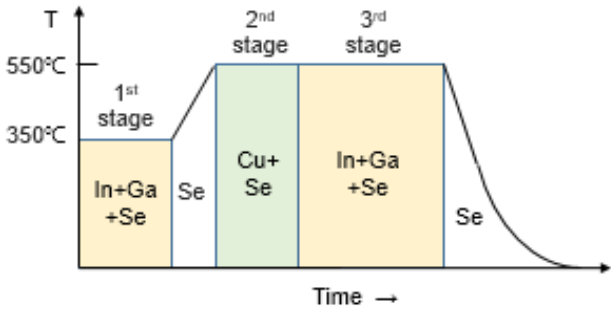

Fig. 2. Schematic profile of β-CIGS film growth.

we characterized β-CIGS based on the Se variation near the surface and correlated it to the cell performance. This is a more detailed study of Se variation compared to the previous report in the literature[12]. It was reported that Na_2S post deposition treatment (PDT) enhanced the cell efficiency to above 19% in α-CIGS solar cell[13]. We also applied Na_2S PDT to an optimized β-CIGS cell for possible higher efficiency.

2. Experimental

2.1 Film fabrication

Fig. 2 shows the schematic temperature profile for the film growth. A polycrystalline β-CIGS absorber layer was prepared on a Mo-coated soda lime glass (SLG) substrate by a three-stage co-evaporation process. In the first stage, an $(In,Ga)_2Se_3$ film was deposited at 350°C by co-evaporating In, Ga, and Se. In the second stage, Cu and Se were supplied by evaporation to form a $Cu(In,Ga)Se_2$ (α-CIGS phase) at 550°C. In the third stage, In, Cu, and Se sources were co-evaporated on the CIGS films to convert them to a β-CIGS phase. The samples were then cooled to 350°C in a Se atmosphere and further cooled without a Se supply.

The thickness of the absorber layer was controlled to 2 μm and the evaporation rates of Cu, In, Ga, and Se were 1.0, 3.0, 2.5 and 14 Å/s, respectively. The Se content of the CIGS film was varied by applying a lower Se flux (11 Å/s) at the third stage with various supply times, for example, 20, 40, 60, 80, and 100% of the third-stage elapse time. The Se crucible temperatures for 14 and 11 Å/s were 280 and 260°C, respectively. Since the Se flux does not represent the composition of the Se in the film due to a low sticking coefficient at 550°C, we measured the Se composition in the film and converted it to a Se/metal ratio as an experimental variable.

2.2 Film Characterization

The surface morphology and microstructure of the β-CIGS films were examined using a field emission scanning electron microscope (FE-SEM) with 5 eV acceleration voltage. Overall elemental compositions were investigated by EDX analysis equipped on a FE-SEM with 20 eV acceleration voltage. The film was confirmed to be β-CIGS phase by Raman spectroscopy analysis. The Raman spectroscopy measurement was carried out with a dispersive Raman spectrometer at 633 nm.

The Cu/(Ga+In) (CGI) and Ga/(Ga+In) (GGI) ratios of the β-CIGS films, determined by energy dispersive spectroscopy (EDS), were approximately 0.36 and 0.41, respectively, resulting in $Cu_{1.08}(In_{0.59}Ga_{0.41})_3Sey$, where the y value varies from 4.68 to 5.12.

The chemical states of the films were characterized by X-ray photoelectron spectroscopy (XPS). The XPS spectra and XPS depth profile were taken using a MultiLab 2000 spectrometer equipped with a monochromatic Al Kα (1486.65 eV) X-ray source. The samples were held with Cu clips, which were grounded to the sample stage. For the XPS, the binding energy scales were calibrated using the binding energy position of the C_{1s} core level at 284.5 eV and the ion beam energy was set at 500 eV with a middle current range. Sputtering was carried out by an EX06 argon ion gun and etch levels were 13-15.

The depth profiling data were obtained with time-of-flight secondary ion mass spectroscopy (SIMS, ToF-SIMS55, ION-TOF GmbH, Germany). Bi^+ ions were used as primary ions and positive ions were detected. Sputtering was conducted by using O_2^+ ions with 1 keV ion energy with a 300x300 μm^2 raster size. An area of 100x100 μm^2 was analyzed using Bi^+ ions with 30 keV energy.

2.3 Cell fabrication

The overall configuration of the solar cell was Al-doped ZnO/intrinsic ZnO/CdS/β-CIGS/Mo on a soda-lime glass substrate. The deposited β-CIGS film was annealed at 200ºC for 5 min in a Se environment as a Se post deposition treatment (Se PDT) of the CIGs absorber layer. Then, a CdS buffer layer was deposited by chemical bath deposition using a mixed solution of $CdSO_4$ (0.003 M) in 200 mL DI water, NH_3 (2M) in 60mL of deionized water and CH_4N_2S (0.2M) in 100 mL of deionized water. The samples were then dipped into the chemical bath at 65ºC and held there for 6 min. They were rinsed with deionized water and dried in an oven for 10 min.

60-nm thick Intrinsic ZnO and 350-nm thick Al-doped ZnO films were deposited on to the CdS buffer layer by radio-frequency sputtering with power of 60 W for 70 min and 220 W for 35 min. The sheet resistance of the TCO was 15 Ω/□. An Al electrode was deposited by thermal evaporation of Al through an aperture mask. After Al deposition no further annealing for TCO and the contact was conducted and no antireflective coating was applied.

I-V measurements of the devices with an active area of 0.43 cm^2 were performed with a solar simulator (K3000, McScience) under AM1.5 and 100 mW/cm^2. The solar simulator was calibrated using a standard Si cell.

3. Result and discussion

Fig. 3 shows the Raman spectra of the CIGS film with the compositions of $Cu_{0.9}(In_{0.7}Ga_{0.3})Se_2$ (α-CIGS) and $Cu_{1.1}(In_{0.6}Ga_{0.4})_3Se_5$ (β-CIGS). Structural differentiation between the phases is difficult by x-ray diffraction analysis because of overlap of most peaks. The Raman peak of the A_1 vibration mode of β-CIGS is at 155 cm^{-1}, while that of α-CIGS is located at 174 cm^{-1}. The Raman spectra of α-CIGS with a composition of $Cu_{0.9}(In_{0.7}Ga_{0.3})Se_2$ presented to compare the difference in peak positions. The results show that our film with a composition of $Cu_{1.1}(In_{0.6}Ga_{0.4})_3Se_5$ has only β-CIGS phase. Details of Raman spectroscopy as function of Cu/(In,Ga) ratio was reported in literature 11.

To control the amount of Se in the β-CIGS film, the Se flux was lowered from 15 to 11 Å/s in the middle of the third stage for various times, ranging from 0 to 80% of total time in the third stage process. The composition including Cu/(Ga+In), Ga/(Ga+In), Se, and Se/metal (Se/M) was analyzed by EDS analysis and the

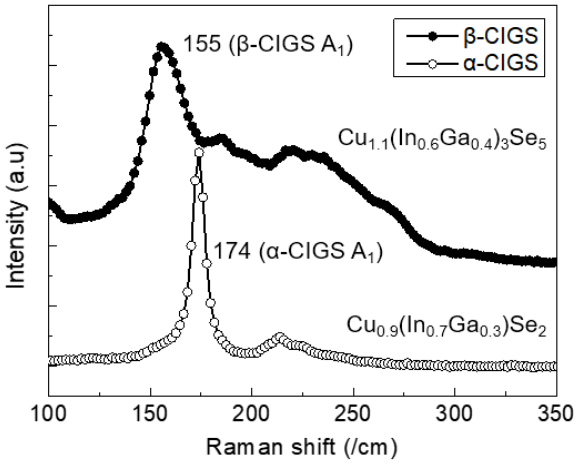

Fig. 3. Raman spectra of α-CIGS and β-CIGS films.

Table 1. Chemical composition analysis of β-CIGS films with various low-Se flux times.

Time (%)	CGI	GGI	Se (%)	Se/metal
0%	0.35	0.40	56.1	1.28
20%	0.37	0.40	55.6	1.25
40%	0.38	0.41	55.3	1.24
60%	0.35	0.42	55.0	1.22
80%	0.35	0.43	54.0	1.17
Aver	0.36	0.41	-	-

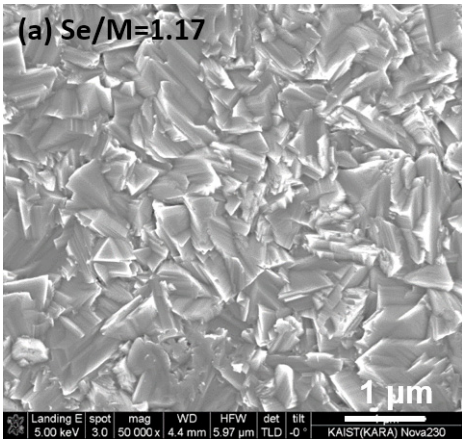

(a) Se/M=1.17

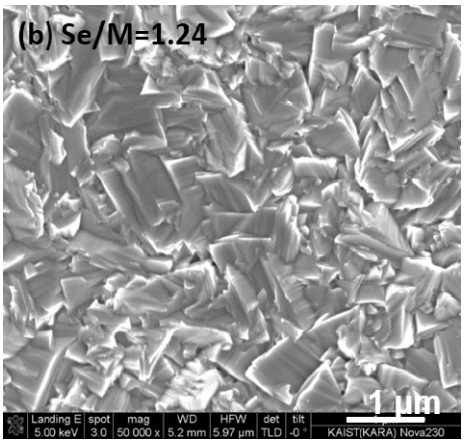

(b) Se/M=1.24

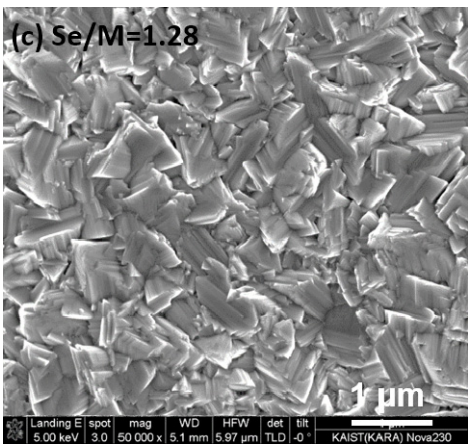

(c) Se/M=1.28

Fig. 4. SEM surface morphologies of films with various Se/M ratios: 1.17 (a), 1.24 (b), and 1.28 (c).

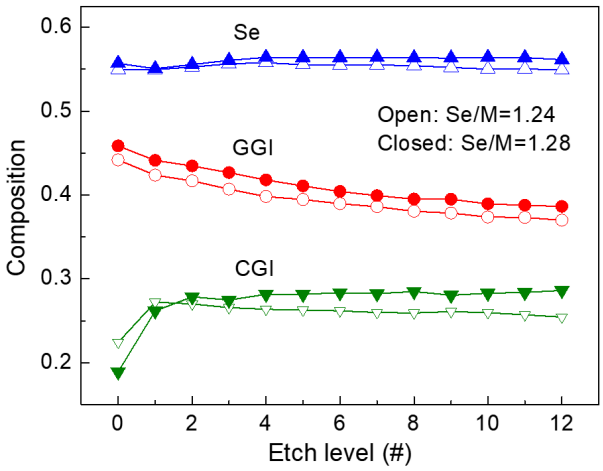

Fig. 5. XPS depth profiles of Se content, Ga/(Ga+In) (GGI) ratio, and Cu/(Ga+In) (GGI) ratio in β-CIGS films for Se/M=1.24 and 1.28.

results are summarized in Table 1. The Se/metal (Se/M) ratio ranged from 1.17 to 1.28, including the stoichiometric value of 1.24.

Fig. 4 shows the plane-view SEM microstructure of the β-CIGS film with Se/M ratios of 1.17, 1.24, and 1.28. The shape of grain boundaries in the film with Se/M=1.17 is curved or round compared to that in the films with Se/M=1.24 and 1.128. For the film with Se/M=1.24, grains are more faceted and grain boundaries are straighter compared to the film with Se/M=1.17. The film with Se/M=1.28 shows a slightly rougher surface with thinner grain edges. It is seen that the film with a stoichiometric composition (Se/M=1.24) has tightly-connected and faceted grains. The film with Se-deficient stoichiometry has curved grain boundaries with less densification and the film with Se-rich stoichiometry has sharper and thinner grains, resulting in a rough surface.

Fig. 5 shows the depth profiles of Cu, In, Ga, and Se elements in the β-CIGS films for Se/M ratios of 1.24 and 1.28. With a higher Se/M ratio of 1.28, the GGI ratio was higher throughout the film and the CGI ratio was also higher throughout the film except very close to the surface.

Fig. 6 shows the current density versus voltage (J-V) curves of β-CIGS solar cells including under AM1.5 illumination. The photovoltaic parameters including short-circuit current (J_{sc}), open-circuit current (V_{oc}), fill factor (FF), and cell efficiency (η) are summarized in Table 2.

The cell with Se/M=1.24 showed the highest conversion efficiency (9.6%) with high V_{oc} and large *FF*, while J_{sc} was low. No antireflective coating layer (ARC) was deposited on the cell.

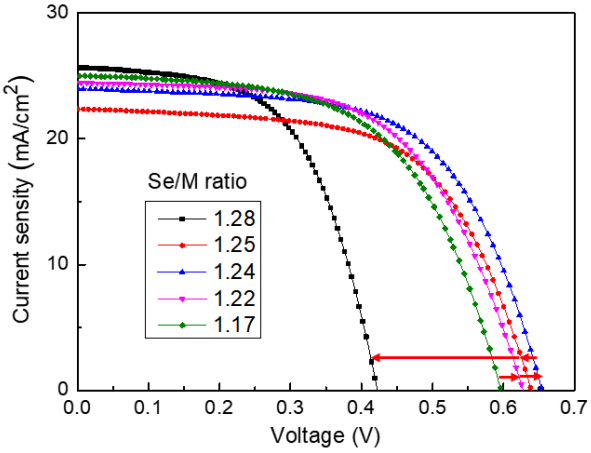

Fig. 6. Illuminated J-V curves of β-CIGS solar cells with various Se/M ratio in the β-CIGS film.

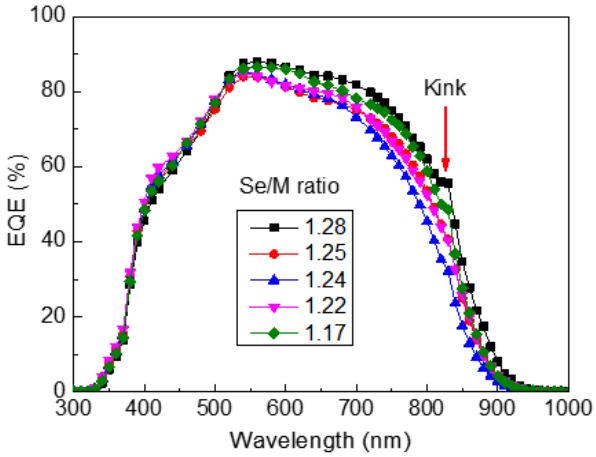

Fig. 7. EQE spectra of β-CIGS solar cells with various Se/M ratio in β-CIGS film.

Table 2. Photovoltaic parameters of β-CIGS solar cells with various Se/M ratio in the β-CIGS film.

Se/M	η (%)	J_{sc} (mA/cm^2)	V_{oc} (V)	FF (%)	R_{sh} ($\Omega \cdot$ cm^2)	R_s ($\Omega \cdot$ cm^2)
1.17	8.6	25.0	0.596	58	1870	1.1
1.22	9.1	24.4	0.628	59	2010	1.3
1.24	9.6	24.0	0.654	61	1180	1.1
1.25	8.7	22.4	0.639	61	1210	1.2
1.28	6.2	25.7	0.422	57	850	0.8

The performance of the cell with various Se/M ratios can be described on the basis of the change of the surface micro-structure.

For the Se/M=1.17 sample, the cell performance was low due to low open circuit voltage and a low fill factor. The surface morphology of the film with Se/M revealed that the grains are not densely packed. With loose connection of grain boundaries, pores developed along the grain boundaries of the film, resulting in deterioration of cell performance. The poor quality of the surface region is thus attributed to an insufficient supply of Se.

For the Se/M=1.24 sample, the CIGS grains on the surface became faceted and tightly connected. Moreover, the CdS/CIGS solar cell showed the best conversion efficiency of 9.6% with J_{sc} = 24.0 mA/cm$_2$, V_{oc} = 0.654 V, and FF = 61.12% in an active area of 0.43 cm^2.

For the Se/M=1.28 sample, V_{oc} and FF were notably low while Jsc was significantly high. Since the surface is rougher with thinner grains, the coverage of CdS on the CIGS surface might be less uniform or less perfect, resulting in a smaller R_{sh} value of 846 Ω/cm^2 while other samples have values on a kΩ /cm^2 scale. As a result, V_{oc} and FF were low. On the other hand, the rough surface can increase the CdS/CIGS junction area and the J_{sc} value can be increased.

Consequently, the Se flux during the third stage of CIGS deposition critically affects the photovoltaic parameters and cell performance. It was found that precise control of Se flux, particularly at the third stage, is critical to obtain reproducible CIGS solar cells. The best performance is expected when the CIGS surface layer is structurally relaxed with well faceted and tightly connected grains.

Fig. 7 shows the external quantum efficiency (EQE) curves of β-CIGS solar cells with various Se/M ratios. In general, the V_{oc} value is lower and the J_{sc} value is larger for a CIGS film with a rougher surface. This is similarly observed in our experiment.

The band gap of the CIGS film with Se/M=1.28 was 1.35 eV, while the band gaps with other Se/M ratios were in a range of 1.41-1.42 eV. The CIGS film with Se/M=1.28 shows a kink in EQE near 820 nm wavelength (1.51 eV) where the absorption loss energy is larger than that of the band gap value. This could be due to inhomogeneity of the CISGS film or Cu contamination into the CdS buffer layer[14], resulting in a noticeable drop of the V_{oc} value. The kink at 820 eV is likely due to Cu contamination in the CdS layer[14]. To avoid Cu contamination, it is necessary to have a CIGS film with densely-packed grains.

Fig. 8 shows the dark current density-voltage (J-V) curves of β-CIGS solar cells with various Se/M ratios. The reverse saturation currents (J_o) of CIGS cells with Se/M=1.17, 1.22, 1.24, 1.25, and 1.28 were 3.6x10^{-7}, 3.3x10^{-5}, 5.5x10^{-7}, 1.1x10^{-5}, and 1.0x10^{-6}, respectively. The relation between V_{oc} and J can be expressed as V_{oc}= kT/q ln(J_{sc}/J_o). In our experiment this relation did not appear to hold due to low cell efficiency. But it is clear that a large V_{oc} is obtained when the Jo value is below an order

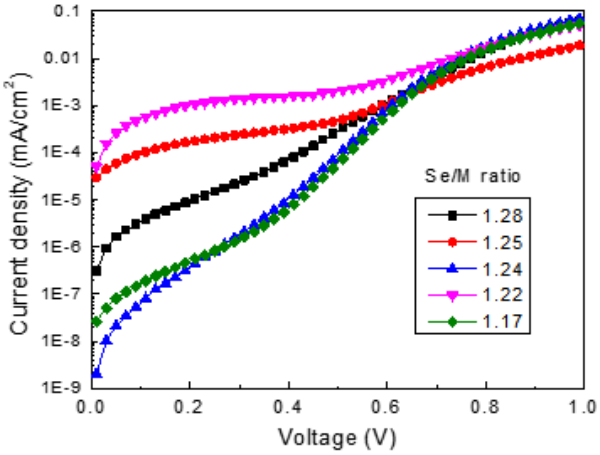

Fig. 8. Dark J-V curves of β-CIGS solar cells with various Se/M ratio in β-CIGS film.

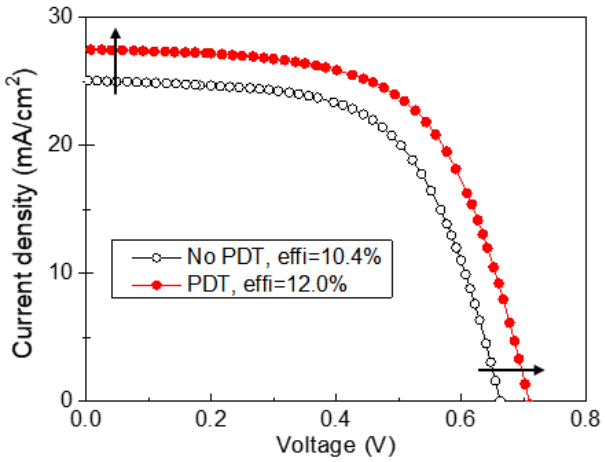

Fig. 9. Illuminated J-V curves of β-CIGS solar cells with and without Na_2S PDT of β-CIGS film.

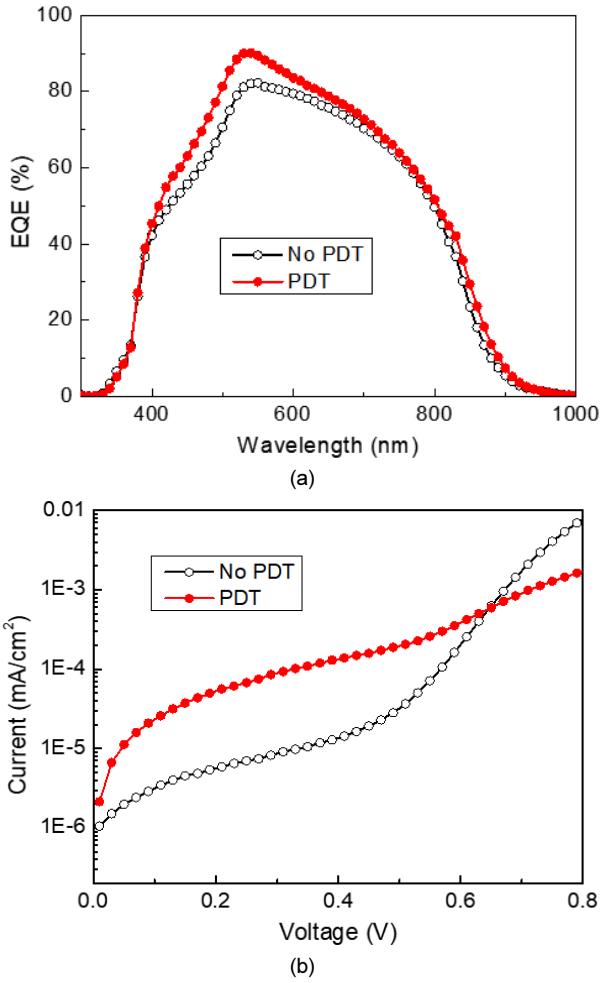

Fig. 10. EQE spectra (a) and dark J-V curves of β-CIGS cell with and without Na_2S PDT for β-CIGS film.

of 10^{-6} Ω·cm^2.

Na_2S PDT treatment greatly enhanced the cell performance in the α-CIGS solar cell up to 19.2%[13]. Na2S PDT was more effective to enhance the cell performance compared to NaF PDT, where cell efficiency of 17.9% was achieved without an antireflective coating[15]. Therefore, we applied the same PDT treatment to the β-CIGS film. A 15-nm thick Na_2S layer was deposited on a β-CIGS film with a deposition rate of 0.5 Å/s. The optimum annealing temperature and the time for Se annealing were 250ºC and 15 min, respectively.

Fig. 9 shows the J-V curves of the β-CIGS solar cells with and without Na_2S PDT under the optimum annealing conditions. No antireflective coating layer was applied. The cell efficiency increased from 10.4% to 12.0% by the Na_2S PDT process. The V_{oc}, J_{sc}, and FF of the CIGS cell without PDT were 0.663 V, 24 mA/cm^2, and 0.62, respectively. The corresponding values for the CIGS solar cell with Na_2S PDT were 0.709 V, 27.5 mA/cm^2, and 0.61, respectively. It is noted that, by the PDT process, the V_{oc} and J_{sc} values were greatly increased while the FF value was nearly the same. Furthermore, the R_{sh} value increased from 1.5 to 2.2 kΩ·cm^2 and the J_o value was lowered from $2x10^{-6}$ to $5x10^{-10}$ A/cm^2.

In α-CIGS, Na_2S PDT introduced a surface layer with a lower valence-band maximum that prevents holes from passing across the CdS buffer layer[15]. The same explanation could be applied to β-CIGS, but a detailed analysis is beyond the scope of this paper. It is believed that the cause of the increase of Jsc and Voc in β-CIGS with Na_2S PDT is the same as that in α-CIGS with Na_2S PDT.

Fig. 10 shows the EQE curves (a) and dark J-V curves (b) of β-CIGS cells with and without Na_2S PDT. In the EQE curves it is seen that the increase of the Jsc value was due to the EQE enhancement near the blue-wavelength region, suggesting that

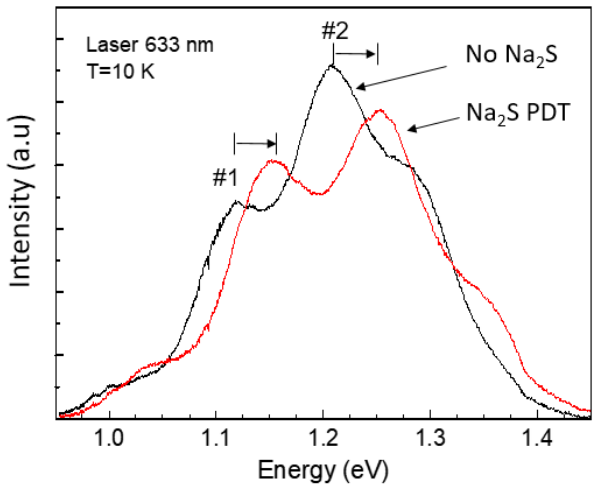

Fig. 11. Photoluminescence spectra of β-CIGS films with and without Na_2S PDT.

the CdS/CIGS interface was much sturdier as a result of the Na_2S PDT process. In the dark J-V curves the Jo value was substantially lowered after the Na_2S PDT process. This suggests that the junction barrier was greatly increased and surface recombination was significantly suppressed by the Na_2S PDT. Our results indicated that the formation of a surface layer with a lower valence band maximum was also effective for the β -CIGS layer film.

Fig. 11 shows the photoluminescence spectra of β-CIGS with and without the Na_2S PDT process, measured at 10K. In the CIGS film without Na_2S PDT, two prominent peaks appeared at 1.12 and 1.21 eV, which were denoted as #1 and #2 peaks, respectively. It is believed that the dominant peaks appear due to strong donor-acceptor recombination. The types of donors are not well understood yet. At the moment we can speculate that peak #1 is due to electron recombination from In-in-Cu sites (In_{Cu}) to Cu vacancy (V_{Cu}) site and peak #2 can be assigned to electron recombination from Se vacancy-Cu vacancy (V_{Se}-V_{Cu}) pair defects at the V_{Cu} site.

It is noted that these peaks shifted to 1.15 and 1.25 eV after Na_2S PDT with a 40-meV difference. The 40 meV shift is close to the ionization of Cu vacancies in the CIGS film. The results suggest that Cu vacancies were eliminated at the CIGS surface layer by Na_2S PDT and the recombination mechanism changed from donor to valence band recombination. From PL information it is seen that the Cu concentration is largely eliminated and Cu vacancies are similarly eliminated. This indicates that a surface layer with Cu-depletion was formed by the Na_2S PDT process on the surface of the β-CIGS film, as in the α-CIGS film.

However, the efficiency achieved by Na_2S PDT was still lower than the 14.2% efficiency in the β-CIGS cell where Na_2S was incorporated at 550ºC[15]. From our results, to achieve efficiency above 14.2%, it is necessary to conduct both Na_2S incorporation at 550ºC and Na_2S PDT at 250ºC. However, such work is beyond the scope of this paper.

4. Conclusions

$Cu(In,Ga)_3Se_5$ (β-CIGS) phase is known to exist at the surface of β-CIGS films to achieve high-performance cell performance. But the cell performance of β-CIGS itself has not been intensively studied. Previously we reported on the effect of Cu and Ga content on the cell performance of β-CIGS phase.

In this paper we reported the effect of Se content as a function of Se/M ratio on the cell performance of β-CIGS phase. Among various Se/M ratios, it was found that the Se/M=1.24, that which is was the stoichiometric composition for the phase, provided a dense connection of densely connected grains and a smooth film morphology. As a result, the cell performance was the best with an efficiency of 9.6%.

To further enhance the cell performance, we conducted Na_2S PDT in β-CIGS. With the Na_2S PDT the cell performance was increased to 12.4% when the PDT was conducted at 250ºC for 15 min. We found that alkali PDT was also available to β-CIGS as well as α-CIGS. Given that our previous result of 14.2 % was achieved with Na_2S incorporation at 550ºC[16], the present Our results suggest that, since our previous result with 14.2 % was achieved by Na_2S incorporation at 550ºC[16], it is necessary to combine Na_2S incorporation at 550C and Na_2S PDT at 250ºC should be combined for higher efficiency.

Acknowledgments

This work was financially supported by the Technology Development Program to solve climate change from the National Research Foundation (NRF) of Korea (2016M1A2-A2936757) and by the Korea Institute of Energy Technology Evaluation and Planning (KETEP) (No. 20163030013690).

References

1. Jackson, P., Wuerz, R., Hariskos, D., Lotter, E., Witte, W., Powalla, M., "Effects of heavy alkali elements in $Cu(In,Ga)Se_2$ solar cells with efficiencies up to 22.6%" Phys. Status. Solidi.

RRL, Vol. 10, pp. 583-586, 2016.

2. Wu, J. L., Hirai, Y., Kato, T., Sugimoto, H., Bermudez, V., "New world record efficiency up to 22.9% for Cu(In,Ga)(Se,S)$_2$ thin film solar cell", 7th World Conference on Photovoltaic Energy Conversion (WCPEC-7), Waikoloa, Hawaii, USA, June 10-15, 2018.
3. Kwon, S. H., Ahn, B. T., Kim, S. K., Yoon, K. H., Song, J., "Growth of $CuIn_3Se_5$ layer on $CuInSe_2$ and its effect on the photovoltaic properties of In_2Se_3/$CuInSe_2$ solar cells", Thin. Solid Films, Vol. 323, pp. 265-269, 1998.
4. Kwon, S. H., Park, S. C., Ahn, B. T., Yoon, K. H., Song, J., "Effect of $CuIn_3Se_5$ layer thickness on $CuInSe_2$ thin films and devices", Solar Energy, Vol. 64, pp. 55-66, 1998.
5. Lee, D. Y., Yun, J. H., Yoon, K. H., Ahn, B. T., "Characterization of Cu-poor surface on Cu-rich $CuInSe_2$ thin film prepared by evaporating binary selenide compounds and its effect of solar efficiency", Thin. Solid Films, Vol. 410, pp. 171-176, 2002.
6. Shin, Y. M., Lee, C. S., Shin, D. H., Kwon, H. S., Park, B. G., Ahn, B. T., "Surface modification of CIGS film by annealing and its effect on the band structure and photovoltaic properties of CIGS solar cells", Curr. Appl. Phys., Vol. 15, pp. 18-24, 2015.
7. Nishimura, T., Toki, S., Sugiura, H., Nakada, K., Yamada, A., "Interfacial quality improvement of Cu(In,Ga)Se_2 thin film solar cells by Cu-depletion layer formation", Appl. Phys. Express, Vol. 9, p. 092301, 2016.
8. Paszkowicz, W., Lewandowska, R., Bacewicz, R., "Rietveld refinement for CuInSe2 and CuIn3Se_5", J. Alloys Compd. Vol. 362, pp. 241-247, 2004.
9. Yamazoe, S., Kou, H., Wada, T., "A structural study of Cu-In-Se compounds by x-ray absorption fine structure", J. Mater. Res., Vol. 26, pp. 1504-1516, 2011.
10. Maeda, T., Gong, W., Wada, T., "Crystallographic and optical properties and band structures of $CuInSe_2$, $CuIn_3Se_5$, and $CuIn_5Se_8$ phases in Cu-poor Cu_2Se-In_2Se_3 pseudo-binary system", Jpn. J. Appl. Phys., Vol. 55, p. 04ES15, 2016.
11. Kim, J. H., Shin, Y. M., Kim, S. T., Kwon, H. S., Ahn, B. T., "Fabrication of wide-band Cu(In,Ga)$_3Se_5$ thin films and their application to solar cells", Curr. Photovolt. Res., Vol. 1, pp. 38-43, 2013.
12. Kim, J. H., Cha, E. S., Park, B. G., Ahn, B. T., "Effect of Se flux and Se treatment on the photovoltaic performance of β-CIGS solar cells", Curr. Photovolt. Res., Vol. 3, pp. 39-44, 2015.
13. Kim, S. T., Larina, L., Yun, J. H., Shun, B., Ahn, B. T., "Surface passivation and point defect control in Cu(In,Ga)Se_2 film with a Na_2S deposition treatment for higher than 19% cell performance", Sustainable Energy & Fuels, Vol. 3, pp. 709-716, 2019.
14. Ahn, B. T., Yun, J. H., Cha, E. S., Park, K. C., "Understanding the degradation mechanism in CdS/CdTe solar cells using a Cd-deficient CdTe layer", Curr. Appl. Phys., Vol. 12, pp. 174-178, 2012.
15. Kim, S., Ko, Y. M., Kim, S. T., Choi, Y. W., Park, J. K., Ahn, B. T., "Reduction of point defects and Cu surface composition in Cu(In,Ga)Se_2 film by Se annealing with a NaF over layer at intermediate temperature", Curr. Appl. Phys., Vol. 17, pp. 820-828, 2017.
16. Kim, J. H., Kim, S. T., Larina, L., Ahn, B. T., Kim, K. H., Yun, J. H., "Increase in conversion efficiency of above 14% in Cu(In,Ga)$_3Se_5$ (β-CIGS) solar cells by Na_2S incorporation through the surface of β-CIGS film," Sol. Energy Mater. Sol. Cells, Vol. 179, pp. 289-296, 2018.